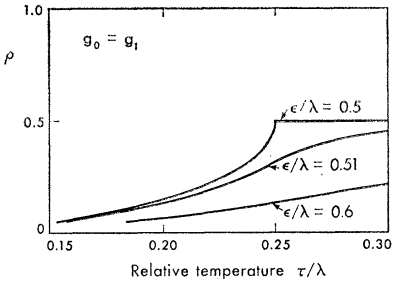

FIG. 4. Order parameter for $g_0=g_1$ for second-order transition with $\epsilon/\lambda=0.50$. For $\epsilon/\lambda=0.51$ and (0.60) there is no transition.

difference. Thus we may write, with α a constant,

$$U=-\tfrac{1}{2}N\alpha(1-2\rho)^2=-\tfrac{1}{2}N\alpha(1-4\rho+4\rho^2). \quad (21)$$

On comparison with (3) we see that

$$\epsilon=2\alpha; \quad \lambda=4\alpha, \quad (22)$$

so that (19) and (20) are consistent and give $\beta_c\alpha=1$. An example of a second-order transition is shown in Fig. 4 for $\epsilon/\lambda=0.5$.

No transition. We see from (6) and Fig. 1 that there is no transition if $\beta(\epsilon-\lambda\rho)+\ln(g_0/g_1)$ intercepts the horizontal axis to the right of $\rho=\frac{1}{2}$, for then ρ as determined by (6) will approach the value $\frac{1}{2}$ smoothly as $\tau\rightarrow\infty$. Thus there is *no transition* if at $\rho=\frac{1}{2}$ the left-hand side of (6) is positive, so that

$$\ln(g_0/g_1)>0 \quad (23)$$

or

$$g_0>g_1. \quad (24)$$

Summary.

(a) A necessary condition for a transition to occur on our model is that the degeneracy g_1 of the excited state be higher than the degeneracy g_0 of the ground state; otherwise, no transition occurs.

(b) *A second-order transition* occurs at $kT_c=\frac{1}{4}\lambda$, but only if $\epsilon=\frac{1}{2}\lambda[1+\frac{1}{2}\ln(g_1/g_0)]$.

(c) A *first-order transition* occurs at

$$kT_c=(\epsilon-\tfrac{1}{2}\lambda)/\ln(g_1/g_0), \quad (25)$$

provided that $\epsilon<\frac{1}{2}\lambda[1+\frac{1}{2}\ln(g_1/g_0)]$, supposing always that $\frac{1}{2}\lambda<\epsilon$. We have a supertransition if $\epsilon/\lambda<g_1/(g_0+g_1)$.

PHYSICAL REVIEW VOLUME 139, NUMBER 3A 2 AUGUST 1965

Electronic Structure of Ordered Beta Brass*†

K. H. JOHNSON AND H. AMAR
Temple University, Philadelphia, Pennsylvania
(Received 11 March 1965)

The electronic band structure of ordered beta brass (β' CuZn) has been calculated from first principles by the Green's-function technique. Two slightly different crystal potentials of the muffin-tin type have been tested, both based on free-atom Hartree-Fock wave functions. Each potential has yielded essentially identical results as far as the conduction bands near the Fermi energy are concerned. The difference between the potentials is reflected principally in the location of the d bands relative to the conduction bands. Cross sections of the Fermi surface have been constructed and suggest the presence of a surface which can be generated by small modifications of the one-orthogonalized-plane-wave prototype. The first (cubic) Brillouin zone is full except for holes in the corners, and the second (dodecahedral) zone is somewhat more than half full with measurable contact of the Fermi surface with the {110} faces of this zone. These observations agree quantitatively with the interpretation of presently available de Haas–van Alphen data. Optical transitions responsible for the color of the alloy have been tentatively identified as occurring over an energy range of 2.5 to 3.5 eV, from the Fermi surface to higher unoccupied levels. The band structure is also compared with the results of electronic-specific-heat, Hall-effect, and elastic-modulus experiments. A band calculation of the cellular type has been carried out separately and compared with the Green's-function bands. The stability of the beta phase is discussed in terms of the Fermi surface, and is related to the present understanding of Cu and of other alloy phases of the CuZn system.

I. INTRODUCTION

THE electronic band structures of many simple metals, such as the alkalis, Cu, Zn, and Al, have recently been determined to a relatively high degree of accuracy, thus leading to a rather satisfactory understanding of many of the properties of these elements. On the other hand, no full-scale theoretical investigation of metallic alloys has been performed, although the latter have been the objects of several qualitative remarks and conjectures. We have been concerned in our laboratory with an experimental and theoretical study of binary beta-phase alloys belonging to groups IB and IIB of the periodic table, including βCuZn (beta brass), βAgZn, βAgCd, βAuZn, and βAuCd. This has led us

* Supported by the U. S. Atomic Energy Commission.
† This work is included in a thesis submitted by K. J. in partial fulfillment of the requirements of the Ph.D. degree at Temple University.

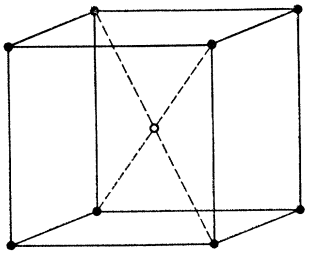

FIG. 1. CsCl type of unit cell characterizing stoichiometric ordered beta brass ($\beta'Cu_{50}Zn_{50}$). At room temperature the ordered phase is observed over the composition range $\beta'Cu_{56}Zn_{44}-\beta'Cu_{48}Zn_{52}$. At temperatures of 454°C (Cu-rich side) and 468°C (Zn-rich side), the alloy disorders into the bcc structure.

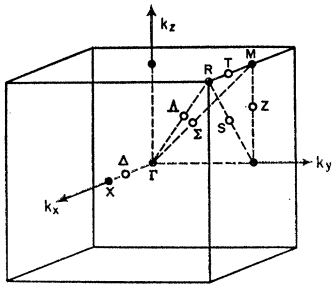

FIG. 2. Simple cubic Brillouin zone for ordered beta brass. The basic symmetry directions and points are shown.

naturally to undertake the calculation of the electronic structure of ordered beta brass, the prototype of this family of alloys. We present in this paper the results of our calculation and their physical implications.

At room temperature these alloys are ordered in the β' phase, which is characterized by the CsCl type of structure (see Fig. 1) and a relatively narrow range of atomic composition in the vicinity of the $\beta'X_{50}Y_{50}$ stoichiometry. These alloys disorder to the bcc β phase at high temperatures, and are prone to martensitic transformations. The Brillouin zone for the ordered alloy is simple cubic and is illustrated in Fig. 2. We have chosen β'CuZn for detailed study, first of all, because of the availability of experimental information. Muldawer[1] has observed that the alloy exhibits rather distinct color variations as a function of both composition and temperature. Johnson and Esposito[2] have shown that these optical properties can be explained in terms of interband transitions and plasma oscillations. Springford, Pearson, Jan, and Templeton[3] have recently studied the Fermi surface of stoichiometric beta brass using the de Haas–van Alphen effect. Measurements of the electronic specific heat,[4] Hall effect,[5] elastic moduli,[6] and extended studies of the optical properties[7] have also been carried out. Secondly, a knowledge of the band structure of this alloy is of intrinsic interest. It is a compound of two metals whose individual band structures and Fermi surfaces are well understood. Zn exhibits a decidedly nearly free-electron band structure and Fermi surface,[8] while Cu departs markedly from such behavior.[9,10] Finally, among the beta-phase alloys, β'CuZn is least subject to relativistic corrections of the band structure.

The Green's-function method has been found to be the most appropriate one for our problem. Sharing with the augmented-plane-wave (APW) method a relatively rapid degree of convergence, it has the additional feature that the largest computational effort, namely, the determination of certain lattice sums (structure constants), can be utilized in similar band calculations of other materials having the same crystal structure. The Green's-function approach to band structure was first formulated in two alternative but equivalent forms by Korringa[11] (partial waves) and by Kohn and Rostoker[12] (variational principle). Raychaudhuri[13] and Segall[14] discussed its possible extension to lattices having more than one atom per unit cell. Morse[15] and Ham and Segall[16] applied the Ewald[17] method to the determination of the structure constants. Using this refinement, Segall computed the bands of Al[18] and of Cu,[9] and Ham[19] computed the bands of the alkali metals.

In the application of the method to a diatomic lattice such as beta brass, certain additional structure constants ("off-diagonal") appear as a consequence of the presence of two atoms per unit cell. Therefore, it has been necessary to modify slightly the structure constants proposed by Ham and Segall in order that these additional constants can be determined. We begin with a brief outline of the main computational steps of the Green's-function technique. For greater detail, the above references, in particular 12 and 16, may be consulted.

II. THE GREEN'S-FUNCTION METHOD

The elements of the fundamental secular determinant of the method can be written in the form

$$\Lambda_{lm;l'm'}{}^{(pq)}(E,\mathbf{k})=\{4\pi\sum_{L,M}D_{LM}{}^{(pq)}(E,\mathbf{k})C_{lm;l'm'}{}^{LM}+(E)^{1/2}\delta_{pq}\delta_{ll'}\delta_{mm'}\cot\delta_l{}^{(p)}(E)\} \quad (1)$$

which clearly reveals the separation of the problem into

[1] L. Muldawer, Phys. Rev. **127**, 1551 (1962).
[2] K. H. Johnson and R. J. Esposito, J. Opt. Soc. Am. **54**, 474 (1964).
[3] M. Springford, W. B. Pearson, J. P. Jan, and I. M. Templeton (private communication).
[4] B. W. Veal and J. A. Rayne, Phys. Rev. **128**, 551 (1962).
[5] V. Frank, Danske Videnskab. Selskab, Math.-Fys. Medd. **30**, No. 4 (1955).
[6] G. M. McManus, Phys. Rev. **129**, 2004 (1963).
[7] L. Muldawer (private communication).
[8] W. A. Harrison, Phys. Rev. **126**, 497 (1962).
[9] B. Segall, Phys. Rev. **125**, 109 (1962).
[10] G. A. Burdick, Phys. Rev. **129**, 138 (1963).
[11] J. Korringa, Physica **13**, 392 (1947).
[12] W. Kohn and N. Rostoker, Phys. Rev. **94**, 1111 (1954).
[13] A. Raychaudhuri, Z. Physik **148**, 435 (1957).
[14] B. Segall, Phys. Rev. **105**, 108 (1957).
[15] P. M. Morse, Proc. Natl. Acad. Sci. U. S. **42**, 276 (1956).
[16] F. S. Ham and B. Segall, Phys. Rev. **124**, 1786 (1961).
[17] P. Ewald, Ann. Physik **49**, 117 (1916).
[18] B. Segall, Phys. Rev. **124**, 1797 (1961).
[19] F. S. Ham, Phys. Rev. **128**, 82 (1962).

two parts: that part which depends only on the crystal structure through the structure constants $D_{LM}^{(pq)}(E,\mathbf{k})$, and that part which depends only on the crystal potential through the partial wave scattering phase shifts $\delta_l^{(p)}(E)$. For each chosen point $\mathbf{k}$ of the Brillouin zone, the zeros of the determinant, properly interpreted, yield a set of eigenenergies $E_1(\mathbf{k})$, $E_2(\mathbf{k})$, $\cdots$.

The nature of our problem requires a large number of structure constants for the CsCl type of lattice. Those constants computed by Segall and Ham[20] are for simple fcc and bcc lattices, and, therefore, are not applicable to our case. The constants originate as coefficients in the expansion of the Green's function in spherical harmonics. In the Ewald type of formulation, they take the form of sums over the direct lattice vectors $\mathbf{R}_n$ and reciprocal lattice vectors $\mathbf{K}_n$. For a complex lattice with a basis having a unit cell of volume τ in which atoms p and q are connected by the vector $\mathbf{a}_{pq}$, each structure constant is equal to the sum of the three quantities (using essentially the notation of Ham and Segall[16])

$$D_{LM}^{(pq)(1)}=(4\pi/\tau)(E)^{-L/2}\exp(E/\eta)\times\sum_n\frac{|\mathbf{k}+\mathbf{K}_n|^L\exp[i(\mathbf{k}+\mathbf{K}_n)\cdot\mathbf{a}_{pq}]}{E-(\mathbf{k}+\mathbf{K}_n)^2}\times\exp[-(\mathbf{k}+\mathbf{K}_n)^2/\eta]Y_{LM}(\mathbf{k}+\mathbf{K}_n),$$

$$D_{LM}^{(pq)(2)}=\pi^{-1/2}(-2)^{L+1}i^L(E)^{-L/2}\sum_n{}'\,|\mathbf{R}_n-\mathbf{a}_{pq}|^L\times\exp(i\mathbf{k}\cdot\mathbf{R}_n)Y_{LM}(\mathbf{R}_n-\mathbf{a}_{pq})\int_{\frac{1}{2}\eta^{1/2}}^{\infty}\xi^{2L}\times\exp[(E/4\xi^2)-(\mathbf{R}_n-\mathbf{a}_{pq})^2\xi^2]d\xi, \quad (2)$$

$$D_{LM}^{(pq)(3)}=-\delta_{pq}\delta_{L0}\delta_{M0}\frac{\eta^{1/2}}{2\pi}\sum_{m=0}^{\infty}\frac{(E/\eta)^m}{m!(2m-1)},$$

in which η is a parameter which is adjusted for maximum rate of convergence of the sums. The on-diagonal ($p=q$) constants reduce to those described by Ham and Segall for monatomic unit cells. In the second summation, the $\mathbf{R}_n=0$ term is to be omitted for the on-diagonal case. The constants have been programmed and computed on an IBM 7094 computer over a wide range of parameters E, L, and M for $\mathbf{k}$ points along the principal symmetry directions of the cubic zone. The quantities $C_{lm;l'm'}{}^{LM}$ are integrals over triple products of spherical harmonics and have been tabulated by Ham.[21]

The phase shifts are defined through the relation

$$\cot\delta_l^{(p)}(E)=\left[\frac{n_l'(\kappa r_p)-n_l(\kappa r_p)L_l^{(p)}(E,r_p)}{j_l'(\kappa r_p)-j_l(\kappa r_p)L_l^{(p)}(E,r_p)}\right]\Bigg|_{r_p=b_p} \quad (3)$$

in which $L_l^{(p)}(E,r_p)$ is the logarithmic derivative of the lth-order radial component $R_l^{(p)}(E,r_p)$ in the expansion of the wave function around atom p,

$$\psi(\mathbf{k}^\alpha;E,\mathbf{r})=\sum_{l,\gamma}^{l_{\max}}i^lC_{l\gamma}{}^{(p)\alpha}R_l^{(p)}(E,r_p)K_{l\gamma}{}^\alpha(\mathbf{r}_p). \quad (4)$$

In the last expression, $K_{l\gamma}{}^\alpha(\mathbf{r}_p)$ is the real lattice harmonic of lth degree which transforms according to the αth irreducible representation of the group of $\mathbf{k}$. It is given, in turn, by a linear combination of spherical harmonics

$$K_{l\gamma}{}^\alpha(\mathbf{r})=\sum_m a^{(p)\alpha}{}_{lm;\gamma}Y_{lm}(\mathbf{r}). \quad (5)$$

For $\mathbf{k}$ points on the faces of the cubic zone, an irreducible representation appropriate to the expansion around atom p is different from, but related to, that appropriate to the expansion about atom q. The radial functions are obtained by integrating the radial equation

$$\left[-\frac{1}{r_p{}^2}\left(\frac{d}{dr_p}\right)r_p{}^2\left(\frac{d}{dr_p}\right)+\frac{l(l+1)}{r_p{}^2}+V(r_p)-E\right]\times R_l^{(p)}(E,r_p)=0 \quad (6)$$

for the chosen muffin-tin crystal potential $V(r_p)$ (see below) over a range of energies, subject only to the condition that the solutions be finite at the origin. The radial functions are then interpolated to their values at the radius b_p of the muffin-tin sphere surrounding atom p, and their first derivatives computed. Finally, the resulting logarithmic derivatives along with the spherical Bessel functions $j_l(\kappa r_p)$, their derivatives $j_l'(\kappa r_p)$, the spherical Neumann functions $n_l(\kappa r_p)$, and their first derivatives $n_l'(\kappa r_p)$, all evaluated for $\kappa\equiv E^{1/2}$ and $r_p=b_p$, are substituted into formula (3).

III. CONSTRUCTION OF THE CRYSTAL POTENTIAL

At present there is no definitive yet practicable procedure for constructing a truly self-consistent crystal potential in which the effects of electron-electron and electron-ion correlation are properly included. The Green's-function method requires a muffin-tin approximation to the potential, i.e., one which is spherically symmetric within nonoverlapping spheres centered on the atomic sites and constant elsewhere. Its exact analytical or tabulated form may be determined using in particular our knowledge of the free-atom wave functions, and adapting this information to the lattice under consideration.

The muffin-tin approximation is a reasonable one in the case of beta brass. By virtue of their arrangement in full cubic symmetry, the atoms accomplish a certain degree of natural cancellation of nonspherical contributions in any particular atomic sphere. The spheres have been chosen to be those inscribed to the Wigner-Seitz

[20] B. Segall and F. S. Ham, General Electric Research Laboratory Report No. 61-RL-(2876G), 1961 (unpublished).
[21] F. S. Ham (private communication).

cells of the traditional cellular method (see Fig. 10), and hence are of equal radii for Cu and Zn. This choice is justified because of the gross similarity between the electronic charge distributions of the free atoms.

We have also adopted a Wigner-Seitz-type assumption of the electrical neutrality of each cell. At first sight, the usual argument in its favor (in terms of correlation and exchange) does not stand up as well in the case of the alloy as it does in that of the simple metal, mainly because of the additional $4s$ electron of Zn. However, Mott[22] has shown that if the additional $4s$ electron stays principally near the Zn atom, one may calculate an electrostatic ordering energy which is of the order of magnitude of the measured value. As an upper limit to the ionicity, Mott arrived at net charges of $-0.075e$ and $0.075e$ in the Cu and Zn cells, respectively. Although this amount of ionicity may be important to order-disorder, it is too small to affect the band structure significantly, and so we have neglected it completely. The muffin-tin approximation can then be viewed as a crude treatment of $4s$-$4s$ correlation in the Zn cell. The Zn^{++} ion potential is left completely unscreened, but cut off at the radius of the inscribed sphere.

As a basis for the potential we used the Hartree-Fock free-ion functions of Cu tabulated by Hartree and Hartree[23] and the free-atom functions of Zn due to Piper.[24] The "unavailable" $4s$ function of Cu was obtained by calculating it in the field of the free ion. All functions were renormalized to the equivalent volume sphere, in accord with the assumed neutrality of each cell. The Coulomb contribution to the potential within each cell was determined by evaluating the Hartree integral over the renormalized charge density. The Slater approximation,[25] proportional to the cube root of the charge density, was adopted for the exchange contribution. The resulting potential is plotted in Fig. 3 in terms of the effective charge $2Z_{\text{eff}}(r) = -rV(r)$. Because the Slater approximation is an average one, this crystal potential can be used for all components of the wave functions. The constant value of the potential between muffin-tin spheres has been chosen to be the average of the potential in this region. It is equal to -0.758 Ry.

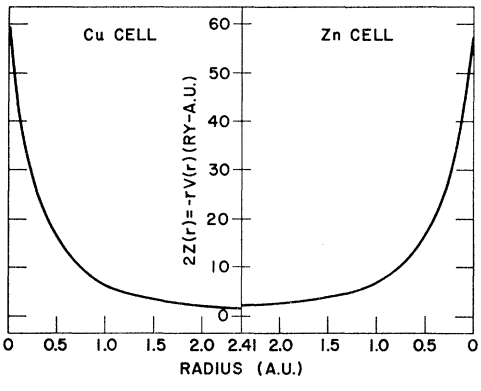

FIG. 3. Muffin-tin crystal potential chosen for $\beta'Cu_{50}Zn_{50}$ and plotted in terms of the "effective charge" within each atomic sphere. The potential is based on the renormalized free-atom wave functions. The Slater free-electron approximation to the exchange potential is used.

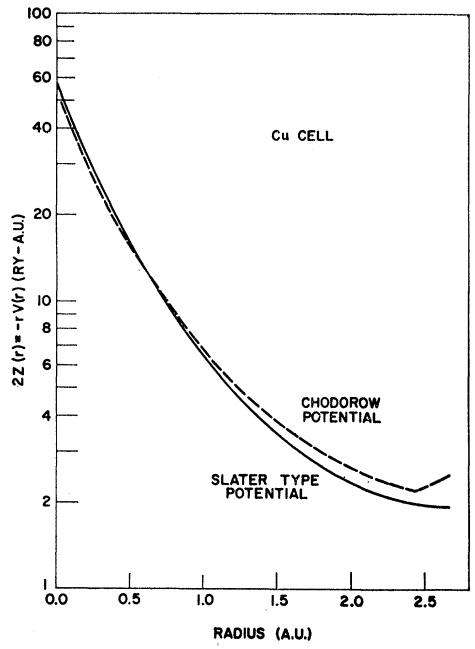

FIG. 4. Comparison of Chodorow potential with potential based on Slater approximation to the exchange for the Cu cell. The former potential is substituted for the determination of $l=2$ components of the Cu wave-function expansions, in order to test the sensitivity of the d bands.

Beside the accurate treatment of correlation, one of the chief uncertainties in the potential is the treatment of the Cu $3d$ electrons. Relative to those of Zn, the Cu $3d$ electrons are rather loosely bound (the atomic $3d$ levels are -0.24 Ry and -0.78 Ry for Cu and Zn, respectively). This difference is reflected in the band structures of the individual metals. In an attempt to study the sensitivity of the bands of β'CuZn to this particular detail, we have adopted a slightly different potential for the $l=2$ component of the Cu wave-function expansions. A potential of the type originally designed by Chodorow,[26] and also used by Segall[9] and Burdick,[10] is purported to be one which more closely approximates the field experienced by a Cu $3d$ electron. It is constructed by first determining the effective potential which yields the free-ion Hartree-Fock $3d$ function when the latter is substituted into the Hartree (without exchange) equation. To this is added the Coulomb potential of a $4s$ wave function calculated in

[22] N. F. Mott, Proc. Phys. Soc. (London) **49**, 258 (1937).
[23] D. R. Hartree and W. Hartree, Proc. Roy. Soc. (London) **A157**, 490 (1936).
[24] W. Piper (private communication).
[25] J. C. Slater, Phys. Rev. **92**, 603 (1953).
[26] M. I. Chodorow, Ph.D. thesis, Massachusetts Institute of Technology, 1939 (unpublished); Phys. Rev. **55**, 675 (1939).

the field of a Cu^+ ion and renormalized to the equivalent volume sphere. The resulting potential is plotted in Fig. 4 as the dashed curve. For the sake of comparison, the Slater-type potential for the Cu cell is shown by the solid curve. The latter potential is used as before for the $l=0, 1, 3, \cdots$ components of the Cu wave functions, and for all the components of the Zn wave functions.

IV. THE CALCULATED BAND STRUCTURE

With the first choice of potential, the bands have been computed for the symmetry points Γ, X, M, and R of the cubic zone (see Fig. 2) and for three points evenly spaced along the symmetry axes Δ, Σ, and Λ. A few conduction levels have also been determined along the edge T of the zone. The convergence of the secular determinants has been very rapid. In the case of the occupied bands, the first one or two nonvanishing terms of the wave functions suffice to yield an accuracy well within the interpolation error of ± 0.005 Ry. For those excited states just above the Fermi level, the first two or three terms are sufficient. The band profiles are illustrated in Fig. 6. They are shown along five directions of the zone and are labeled in the BSW[27] notation. The computed points are indicated by the circles. Where computations at certain interior points have not been carried out, the bands have been sketched on the basis of the compatibility relations and noncrossing rule. The squares indicate levels too close for separation on the graph. The energies at high symmetry points are listed in Table I.

The bands are clearly separated into two parts, namely, the conduction bands which extend upward from the lowest level Γ_1 and the d bands which lie approximately 0.1 Ry below the Γ_1 state. At their widest point R, the latter bands cover an energy of 0.094 Ry. A more narrow set of d levels, not shown in Fig. 6, has been located in the vicinity of the lower energy, -1.75 Ry. The presence of two such d bands is not unexpected. Consider the case where the two atoms of the CsCl-type cell are nearly identical. Then the cell is effectively bcc, and its first zone is a regular dodecahedron. The cubic zone may be taken as a reduced zone for the bcc cell along the $\langle 100 \rangle$ direction. Those sections of the bands between $\mathbf{k}=(2\pi/a)(\frac{1}{2}00)$ and $\mathbf{k}=(2\pi/a)(100)$ of the dodecahedron can be folded into the reduced cubic zone, yielding twice as many bands between $\mathbf{k}=(2\pi/a)(000)$ and $\mathbf{k}=(2\pi/a)(\frac{1}{2}00)$. When the atoms are identical, bands having the same symmetry properties should meet at a common point on the cubic zone boundary. However, when the atoms are different, as in beta brass, the two sets of bands should separate. In the case of the more tightly bound $3d$ electrons, the difference between the bands should be determined largely by the individual atomic term values. Therefore, the d bands shown in Fig. 6 may be attributed principally to the Cu $3d$ electrons and the lower set attributed principally to the Zn $3d$ electrons.

The conduction bands may be compared with those of the empty lattice shown in Fig. 5 along the three principal directions of the zone. Despite sizable splitting of nonessential free-electron degeneracies toward higher energies, the conduction bands at lower energies preserve their nearly free-electron shape. This behavior is also reflected by the relatively small gap between the conduction states $X_{4'}$–X_1 and X_1–$X_{4'}$. It indicates a rather small perturbation at the {100} faces of the zone.

TABLE I. Energies (in rydbergs) for high symmetry points of ordered beta brass. Interpolation error ± 0.005 Ry.

State	$E(\mathbf{k})$, first choice of potential	$E(\mathbf{k})$, second choice of potential
Γ_1	−0.860	−0.860
Γ_{12}	−0.998	−0.638
$\Gamma_{25'}$	−0.971	−0.607
Γ_{15}	+0.219	+0.219
Γ_{12}	+0.482	+0.456
X_1–$X_{4'}$	−0.907	−0.723
X_5–$X_{5'}$	−1.002	−0.645
X_2–$X_{3'}$	−0.988	−0.627
X_3–$X_{2'}$	−0.969	−0.613
$X_{4'}$–X_1	−0.562	−0.545
X_1–$X_{4'}$	−0.536	−0.386
$X_{5'}$–X_5	+0.518	+0.521
M_1–M_3	−1.003	−0.679
M_3–M_1	−0.997	−0.674
M_5–M_5	−0.983	−0.611
M_2–M_4	−0.939	−0.591
$M_{5'}$–$M_{5'}$	−0.333	−0.333
M_1–M_3	−0.076	−0.106
M_3–M_1	−0.065	−0.080
$R_{25'}$–R_{15}	−1.003	−0.678
R_{12}–$R_{12'}$	−0.913	−0.584
R_{15}–$R_{25'}$	−0.021	−0.055
R_1–$R_{2'}$	+0.361	+0.361
$R_{2'}$–R_1	+0.377	+0.377

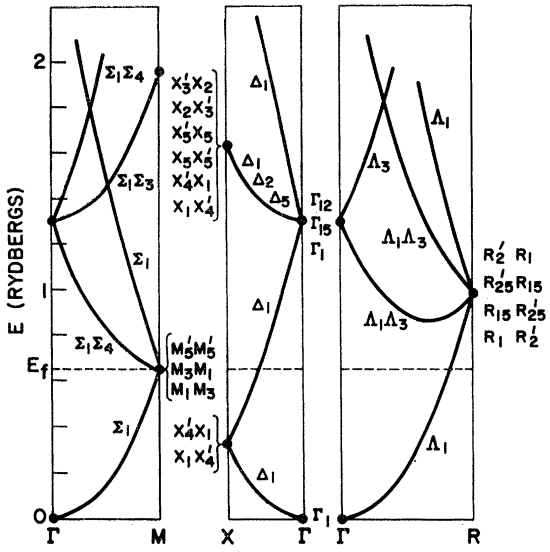

FIG. 5. Free-electron or "empty-lattice" bands along the three principal symmetry axes of the cubic zone. The free-electron Fermi level for ordered beta brass is indicated by the dashed line.

[27] L. P. Bouckaert, R. Smoluchowski, and E. Wigner, Phys. Rev. **50**, 58 (1936).

At points M and R, where planes corresponding to the second (dodecahedral) zone touch the cubic zone, the perturbing effects of the crystal potential are more severe.

The preservation of nearly free-electron character of the lowest parts of the conduction bands is due principally to the relatively low positions of the d bands. This case may be contrasted with that of pure Cu, where overlap between the d bands and conduction bands is responsible for the departure from nearly free-electron behavior. The presence of larger gaps at higher energies in beta brass is not so much dependent upon the relative positions of the d bands, but seems to indicate a trend shared by the band structures of simple metals such as the alkalis[19] and Al.[18]

The conduction levels Γ_1 and Γ_{15} are, respectively, s and p levels because their first nonvanishing wave-function components $l=0$ and $l=1$, respectively, are principally responsible for their positions on the energy scale. In contrast, the lowest M_1–M_3 and X_1–$X_{4'}$ states, for which the first nonvanishing components are s-type, owe their respective positions among the d bands to the dominant effect of their second wave-function component $l=2$. The ordering of conduction states at the zone boundaries is important because it deviates from the normal ordering of levels in the free atom. For instance, $X_{4'}$–X_1 and X_1–$X_{4'}$ are, respectively, p-s and s-p states. $M_{5'}$–$M_{5'}$ is a p level and the M_1–M_3 state above it is an s-d level. R_{15}–$R_{25'}$ is a p-d state and R_1–$R_{2'}$ an s-f state. Similar reversals of order are observed in the bands of many simple metals.

When the Chodorow type of potential is used to calculate the $l=2$ component of the Cu wave functions, the resulting band profiles are those shown in Fig. 7 along the three principal directions of the zone. A comparison with Fig. 6 readily indicates that the chief effect is the expected one, namely, the lifting and widening of the d bands relative to the conduction bands. This behavior is consistent with the tendency of the

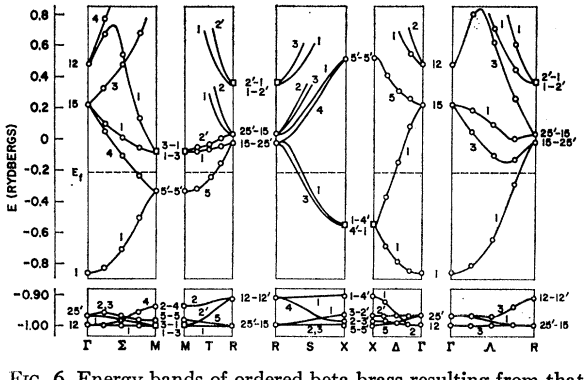

FIG. 6. Energy bands of ordered beta brass resulting from that choice of crystal potential shown in Fig. 3. The bands are indicated for the five principal symmetry directions of the zone. Computed points are represented by the circles. The squares designate two energy levels too close for separation on the graph. The Fermi energy is located by the dashed line.

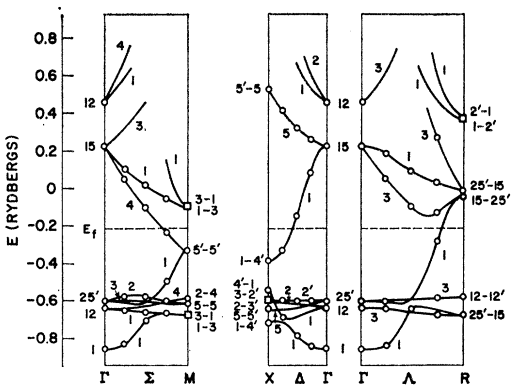

FIG. 7. Energy bands of ordered beta brass resulting when Chodorow potential is used to determine the $l=2$ component of the wave-function expansion around Cu.

Chodorow type of potential to be weaker than the Slater type in the vicinity of the radius 0.6 atomic units (a.u.) where the free-ion $3d$ function peaks. The sensitivity of the d bands to the choice of crystal potential calls attention to the difficulty of constructing a self-consistent potential. A similar sensitivity of the d bands in the case of the transition metals has been discussed by Slater.[28]

The overlap of the d bands with the conduction bands, evident in Fig. 7, is large enough to distort the lowest energy portion from nearly free-electron behavior. The gap separating the $X_{4'}$–X_1 and X_1–$X_{4'}$ states is widened considerably. This is due to the "repulsion" of the $l=2$ component of the upper X_1–$X_{4'}$ level by that of the lowest X_1–$X_{4'}$ level. Despite the presence of $l=2$ components in the wave functions associated with the conduction bands at the Fermi energy and higher (e.g., M_1–M_3), these bands are little changed by the use of the Chodorow potential.

V. THE FERMI SURFACE

In the absence of a sufficiently large number of $E(\mathbf{k})$ values throughout the zone, a direct determination of the density of states and the Fermi energy cannot be carried out to the full limit of accuracy. We have attempted to arrive at an approximate value of the Fermi energy by two alternate methods. In the first of these, a technique originally devised by Houston[29] was borrowed in order to fit a volume element of the Fermi surface to an expansion in lattice harmonics through the sixth degree along the three principal directions of the zone. Using the band profiles of Fig. 6 shown along the Δ, Σ, and Λ directions and requiring the volume of the Fermi surface to contain three conduction electrons per unit cell, we have obtained a value of $E_F=-0.20_5$ Ry. The third decimal place is

[28] J. C. Slater, Quarterly Progress Report, Solid-State and Molecular Theory Group, Massachusetts Institute of Technology, Cambridge, Massachusetts, 1963, No. 51, p. 14 (unpublished).

[29] W. V. Houston, Rev. Mod. Phys. **20**, 161 (1948).

uncertain because of the discontinuity of the Fermi surface across the boundary of the cubic zone into the second (dodecahedral) zone.

An examination of the band profiles in reference to this value of the Fermi energy indicates that the first zone is full except for holes in the corners of the cube. The second zone is slightly more than half full, with a measurable amount of contact of the Fermi surface at the twelve faces of the dodecahedron. These regions of contact can be utilized to determine the Fermi energy by a second method which is similar to that employed by Segall[9] in the case of Cu. It depends on an approximation to the volume of the Fermi surface by that of a sphere of radius roughly equal to the free-electron value, to which is added the volume of the neck regions corrected for the spherical caps enclosed by the necks. The Fermi energy is fixed by requiring this volume to contain the proper number of conduction electrons. In our case we have made use of the band profiles shown in Fig. 6 along directions Σ and T in order to establish the contact area of each neck as a function of $E(\mathbf{k})$. The necks are evidently oval in cross section. We have estimated their areas of contact by assuming them to be ellipses, the major axes of which lie along T and the minor axes along Σ. The resulting Fermi energy is $E_F=-0.21_9$ Ry. The contact area is 0.19 ± 0.02, taking the side of the cube as unity. The mean value of the Fermi energy is indicated by the dashed line in Fig. 6. The same value is indicated for the bands of Fig. 7, although, strictly speaking, it should be computed independently.

We have sketched two important extremal cross sections of the Fermi surface by considering the intersection of the line $E=E_F$ with the band profiles of Fig. 6. In Fig. 8, hole-like orbits in the {110} diagonal plane of the first zone are shown. The corners of these orbits would be considerably sharper in the free-electron limit, and the cross-sectional area would be $A_{110}=0.124$. The calculated area is only 0.083 ± 0.007. The rounded

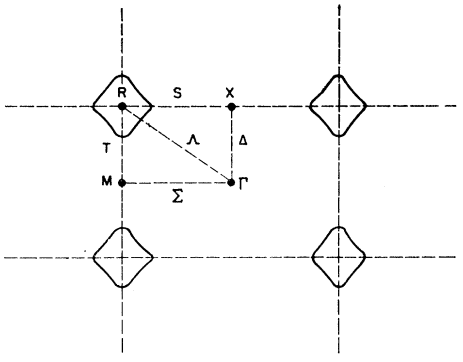

FIG. 8. Hole-like orbits in {110} plane of first (cubic) zone (repeating zone scheme), based on computed bands. The approximate area of each orbit is 0.083 ± 0.007 (taking the side of the cubic zone as unity). This area is considerably less than the free-electron value of 0.124, reflecting both the overlap of the Fermi surface into the second (dodecahedral) zone and its contact with the boundary of the latter.

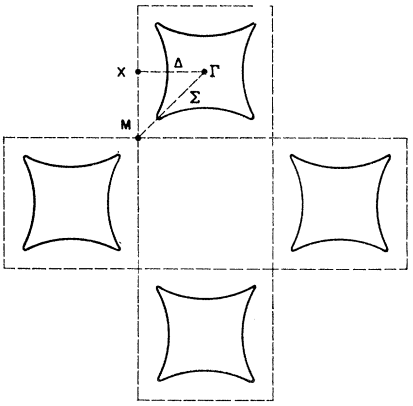

FIG. 9. Hole-like orbits in the {100} plane of the second (dodecahedral) zone (folded into the cubic zone), based on the computed bands. Contact of the Fermi surface with the faces of the dodecahedron is revealed by the rounded corners of each orbit. The "minor neck radius" is given by the intersection of the orbit with the Σ direction.

corners and diminished area are consequences of the perturbing effect of the crystal potential. In Fig. 9 the hole-like orbits are somewhat analogous to the "dog's bone" orbits of Cu in that they clearly indicate the presence of the necks. These orbits lie in the {100} plane of the second zone folded into the first zone.

VI. COMPARISON WITH EXPERIMENT

A. The Fermi Surface

The results of the de Haas–van Alphen experiments[3] on stoichiometric beta brass agree with the assumption that the first zone is simple cubic. They suggest the presence of a Fermi surface which may be generated through reasonable modifications of the nearly free-electron surface at the zone boundaries. Contact at the second zone boundary has also been measured.

As an example of the comparison between experimental and computed results, we may consider the extremal hole-like orbits shown in Fig. 8. The de Haas–van Alphen measurements yield an area of 0.089. This compares well with our computed result 0.083 ± 0.007. Experimental results for the orbits sketched in Fig. 9 are not available. However, Springford[30] has recently determined the neck area and reports a value of 0.17. This may be compared with the theoretical value of 0.19 ± 0.02.

B. The Optical Properties

The characteristic color of beta brass, yellow gold at room temperature, has been shown to be associated with an increase in the absorption coefficient $4\pi k/\lambda$ and the conductivity $nk\omega/2\pi$ in the vicinity of 2.5 eV (4959 Å).[2] Here n and k are, respectively, the real and imaginary parts of the complex refractive

[30] W. Springford (private communication).

index, and ω is the frequency of the incident radiation. Utilizing the band profiles, we have been able to locate an appropriate pair of bands which most likely participate in the transitions, provided the latter are of the direct or "vertical" type. The particular bands are those in the vicinity of the gap between $M_{5'}$–$M_{5'}$ and M_1–M_3 levels. The combined density of states is high in this region, and the Fermi surface contacts the second zone boundary.

At the onset of absorption, those transitions allowed by symmetry together with their vertical gaps are, respectively, $\Sigma_4 \rightarrow \Sigma_1$ (2.23 eV) and $T_5 \rightarrow T_1$ (2.18 eV), i.e., from the Fermi surface to the next unoccupied level. These transitions should continue to occur with increasing probability toward higher energies, as their origin is shifted along the Σ and T directions to the high symmetry point M, where the computed gap is $M_{5'}$–$M_{5'} \rightarrow M_1$–M_3 (3.50 eV). This interpretation is in agreement with the observed increase in optical absorption between 2.5 and 3.5 eV. That the transitions originate from the Fermi surface is further strengthened by the observation of Muldawer[31] that the addition of a small percentage of Zn within the β' field has the effect of shifting the onset of absorption to lower energies. The addition of a small amount of Zn should raise the Fermi surface slightly. If this occurs without appreciably altering the shape of the bands, and the transitions do indeed originate from the Fermi surface, then the threshold energy would be lowered.

Berglund and Spicer,[32] on the basis of photoemission experiments, have recently argued that electronic transitions of the indirect type are very important in Cu and Ag. This is in disagreement with the original interpretation of the optical spectra of these metals by Ehrenreich and Philipp[33] in terms of direct transitions only. The presence of indirect transitions is difficult to ascertain on the basis of conventional optical data. However, we cannot rule out the possibility that such effects may contribute in an important way to the optical properties of β'CuZn. For example, indirect transitions from the Fermi surface to the R_{15}–$R_{25'}$ level would be a distinct possibility. The observed temperature sensitivity of the optical properties, as described by Muldawer,[1] lends some support to the notion that indirect transitions due to electron-phonon coupling may be important in beta brass.

High-energy transitions from the d bands to the Fermi surface would constitute a partial check of the comparative accuracy of the two chosen crystal potentials. The observed difference in the height of the d bands should be optically detectable, provided measurements are made sufficiently far into the ultraviolet. Such measurements are now in progress.[7]

At frequencies lower than those associated with the onset of interband transitions, the optical properties can be described principally by the Drude-Zener model.[34] At such frequencies, usually in the near infrared, the imaginary part of the complex index of refraction has the form

$$k=(4\pi N_c e^2/\omega^2 M_a)^{1/2}\ (\omega\tau\gg 1)\,, \tag{7}$$

where τ is the relaxation time, N_c is the conduction-electron density, and M_a is the average inverse effective mass of the conduction electrons. The last quantity has been defined by Cohen[35] who showed that it can be represented by the formula

$$M_a=\hbar k_F(S_F{}^0/S_F)1/\langle v\rangle_F\,. \tag{8}$$

S_F is the area of the Fermi surface, excluding those parts covered by the zone boundaries. $S_F{}^0$ is the area that the surface would have if it were spherical, namely, $S_F{}^0=4\pi k_F{}^2$, where k_F is the radius of the sphere. $\langle v\rangle_F$ is the velocity of the Bloch electron averaged over the Fermi surface, and is given by

$$\langle v\rangle_F=\frac{1}{\hbar S_F}\int|\nabla_{\mathrm{k}}E(\mathbf{k})|\,dS_F\,. \tag{9}$$

Shulz[36] has measured k/λ of β'CuZn toward the red end of the spectrum, finding a value of 6.05×10^4 cm^{-1}. If we assume relation (7) to be valid in this spectral region, the ratio of conduction-electron density to effective mass is $N_c/M_a=4.11\times10^{22}$ cm^{-3} g^{-1}. On the basis of a density of $N_c=3/a^3$, the mass is $M_a=2.86\,M_0$. Cohen has shown that if interband transitions are lacking in this region, which we believe to be the case in beta brass, then M_a is identical to the optical effective mass.

Utilizing expressions (8) and (9) together with the band profiles of Fig. 6, we have determined an approximate theoretical value of M_a. It was computed by first assuming the Fermi surface to be based upon the sphere whose radius k_F is given by the mean value of the wave vector for the intersection of the line $E=E_F$ with the bands along the Δ and Λ directions. From the area of this sphere were subtracted the areas of twelve spherical caps associated with the contact of the surface at the second zone boundary. To this were added a relatively small correction due to the additional areas of the necks and an even smaller correction due to the gap at the first zone boundary.

In establishing the mean Fermi velocity given by expression (9), we have first assumed the velocity to be constant over the belly regions occupying the corners of the first zone and to be constant, but of slightly different value, over the belly regions of the second zone. The

[31] L. Muldawer (private communication).
[32] C. N. Berglund and W. E. Spicer, Phys. Rev. **136**, A1030 (1964); **136**, A1044 (1964).
[33] H. Ehrenreich and H. R. Philipp, Phys. Rev. **128**, 1622 (1962).
[34] F. Seitz, *The Modern Theory of Solids* (McGraw-Hill Book Company, Inc., New York, 1940), p. 638.
[35] M. H. Cohen, Phil. Mag. **3**, 762 (1958).
[36] Data of L. G. Shulz (unpublished) as reported by J. A. Rayne, in *The Fermi Surface*, edited by W. A. Harrison and M. B. Webb (John Wiley & Sons, Inc., New York, 1960), p. 268.

Δ and Λ profiles were utilized to determine $|\nabla_k E(\mathbf{k})|$ for these two regions. A small correction was added in order to take into consideration the change in velocity in the neck regions. However, this correction is uncertain because of the oval shape of the necks. The optical mass computed on the basis of these approximations has the value of $M_a=(1.8\pm0.2)\ M_0$.

The theoretical value is considerably smaller than that based on optical data. Discrepancies between the theoretical and experimental optical masses, although perhaps not so severe, have been observed in the cases of simple metals, and are usually attributed to the neglect of many-body effects. In the case of beta brass, electron-phonon coupling may be of particular importance. It should be noted that it would take a considerably greater amount of Fermi-surface overlap in order to bring the two values into agreement through formula (8) alone.

C. Electronic Specific Heat

Veal and Rayne[4] have measured the electronic specific heat of beta brass below $T=4.2°$K and over a range of compositions within the β' field. For the $\beta'Cu_{50}Zn_{50}$ composition, the measured value of the coefficient of electronic specific heat is $\gamma=0.699$ mJ mole^{-1} deg^{-2}. The thermal effective mass is defined through the relation

$$M_t/M_0=\gamma/\gamma^0, \tag{10}$$

in which γ^0 is the free-electron limit of γ. With the experimental value of γ and an assumed conduction-electron density of $N_c=3/a^3$, the thermal effective mass is $M_t=1.13\ M_0$.

Veal and Rayne have compared their measurements with a theoretical model based on a nearly free-electron approximation to the band structure. However, they have completely neglected the effect of the first (cubic) zone, and have assumed the Fermi surface to lie continuously within the second (dodecahedral) zone. If we take the bands of Fig. 6 to be an accurate description, then this approximation is not a bad one. For agreement with the measured optical mass, they find a gap of 4.7 eV at each face of the dodecahedron. On the basis of this gap, using a twelve-cone model, these authors have computed a neck radius of 0.530×10^8 cm^{-1} (in the units we have adopted). This may be compared with our computed gap of 3.5 eV and an associated equivalent neck radius of 0.53×10^8 cm^{-1}.

We have calculated the thermal mass on the basis of the band structure by making use of Cohen's[35] formula

$$M_t=\hbar k_F(S_F/S_F{}^0)\langle 1/v\rangle_F. \tag{11}$$

This formula is very similar to (8) and its evaluation has been carried out in essentially the same way, yielding the result $M_t=(0.7\pm0.2)\ M_0$. As in the case of the optical mass, the theoretical value is considerably less than the experimental one. Since the discrepancy is more than likely due to the neglect of many-body effects, an attempt to adjust the energy gaps in order to obtain agreement with the measured thermal mass is not justified.

It has been demonstrated that the ratio of the thermal mass to optical mass should be less than unity when the Fermi surface contacts the zone boundary. The experimental value of this ratio is $M_t/M_a=0.395$. The theoretical value is 0.4. Both values reflect the contact at the second zone boundary. However, their almost exact agreement must be considered as fortuitous, in view of the discrepancies in the masses themselves.

D. Hall Effect

Frank[5] has measured the Hall coefficient of beta brass at low temperature and determined a value of $R=-0.6\times10^{-5}$ cm^3 C^{-1}. The value for pure Cu is $R=-5.2\times10^{-5}$ cm^3 C^{-1}. The fact that the coefficient for the alloy is considerably more positive relative to that for the noble metal can be given the following interpretation. In those regions of the Fermi surface where one or more components of the effective-mass tensor become negative, the Hall coefficient can become more positive without actually involving pure hole conduction in the sense of semiconductor physics. There are more such hole-like regions associated with the Fermi surface of beta brass than with that of Cu, for example, in the corners of the cubic zone (Fig. 8), and in the "pocket" regions where the Fermi surface contacts the second zone boundary (Fig. 9).

E. Elastic Constants

Jones[37] originally suggested that the stability of beta brass can be described in terms of the large contribution to the elastic shear moduli due to contact of the Fermi surface with the (dodecahedral) zone boundary. More recent measurements of the elastic moduli of this alloy as a function of composition by McManus[6] have been interpreted in terms of such Fermi-surface overlap, coupled with second-nearest-neighbor interactions. It has not yet been possible to separate the two contributions and account for their relative magnitudes within the framework of the theory of elastic moduli. Nevertheless, the band-structure results are significant to this theory to the extent of supporting the contention that Fermi-surface overlap is indeed very important in beta brass.

VII. THE CELLULAR CALCULATION

A band calculation of the cellular type[38] has also been carried out for a few energy states of ordered beta brass for the purpose of comparison with the Green's-function results. The cellular method differs from that

[37] H. Jones, Phil. Mag. **43**, 105 (1952).
[38] F. C. Von der Lage and H. A. Bethe, Phys. Rev. **71**, 612 (1947).

of the Green's function in that the Schrödinger equation is solved directly as a boundary-value problem for the chosen atomic polyhedra. In most other respects the two methods have much in common. Thus, a considerable amount of the preparatory work for the Green's-function calculation, such as the choice of atomic cells, choice of crystal potential, radial equation integrations, and construction of symmetry-adapted wave functions can be applied to the cellular calculation.

Of the two methods, the cellular one is least convergent. This is due to the fact that the Bloch conditions are applied directly to the wave-function expansions as boundary conditions at selected points on the faces of the atomic polyhedra. Since these expansions are in terms of products of radial functions and spherical harmonics, they are least convergent at the cell boundary. In other words, we solve the Schrödinger problem as accurately as we can for the chosen potential within each cell, but at the expense of suitably satisfying the boundary conditions.

The calculation has proceeded in the following way. Crystal space was partitioned into Wigner-Seitz cells in the form of truncated octahedra surrounding the atoms (see Fig. 10). The boundary conditions were applied at points located at the centers of the square faces (between like cells), and at points along the circles where the sphere of radius equal to one half the lattice constant intersects the hexagonal faces (between unlike cells). In addition to the application of the boundary conditions at points, the angular parts of the wave functions were expanded in Fourier series in the azimuthal angle α over the aforementioned circles, and the matching carried out in terms of the Fourier coefficients. The latter procedure provides a type of average fitting of the boundary conditions along the circles.

For the maximum number of terms retained in the wave-function expansions (up to $l=8$), there was generally more than one possible set of boundary points. The "best" sets were chosen on the basis of the "empty-lattice test," in which spherical Bessel functions are substituted for the radial functions and the energy eigenvalues are those for free electrons

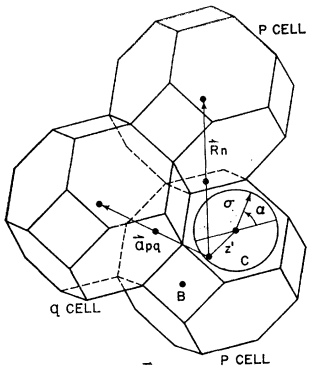

FIG. 10. Wigner-Seitz cells for ordered beta brass. In the cellular calculation, the boundary conditions are applied at points B and at points along the circles C where the sphere of radius equal to one-half the lattice constant intersects the hexagonal faces.

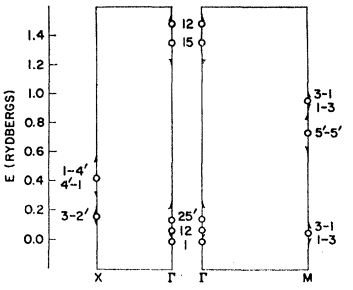

FIG. 11. Energy bands at high symmetry points resulting from the cellular calculation. The energies are measured with respect to the Γ_1 level. The length of each arrow indicates the amount of variation for the particular level at its center, encountered when different sets of boundary points were used.

shown in Fig. 5. The criterion for the test was agreement with these energies to within one or two percent. In a few instances, it was impossible to fulfill this criterion.

The crystal potential shown in Fig. 3 was used to determine the radial parts of the wave functions. The calculation has been carried out for several of the most important levels at the high symmetry points Γ, M, and X. No interior points other than Γ have been considered because of the poor convergence of the method. The results are plotted in Fig. 11. The variation of the computed energies with the choice of boundary points is indicated by the lengths of the arrows. All energies have been measured with respect to the Γ_1 level.

A comparison of Fig. 11 with Figs. 6 and 7 indicates approximate agreement between the cellular and Green's-function results to the extent that the ordering and relative spacing of the levels is similar. In the cellular bands, the d levels lie between those obtained, respectively, for the two choices of crystal potential in the Green's-function calculation. Because of the significant variation of most of the computed eigenenergies with the choice of boundary sets, it must be concluded that the cellular method is not a suitable one for obtaining accurate bands in a compound such as beta brass. The chief importance of such results is the indication of general trends without the necessity of large-scale electronic computers.

VIII. DISCUSSION

The preceding analysis has concerned the electronic structure of ordered beta brass as an ideal metal. It is important that we examine the implications of this analysis on the theory of the beta phase in its relationship to the other phases of the CuZn-alloy system. In their phenomenological theory of the IB–IIB alpha-phase alloys, Cohen and Heine[39] have conjectured that there are two principal effects of alloying on the electronic structure of the parent noble metal. The first is the raising of the energy of the p-like conduction levels and the lowering of the s-like conduction levels at the zone boundary. Since $E_p<E_c$ in pure Cu, the result is to reduce the band gaps in αCuZn, and con-

[39] M. H. Cohen and V. Heine, *Advances in Physics*, edited by N. F. Mott (Taylor and Francis, Ltd., London, 1958), Vol. 7, p. 395.

sequently to "sphericize" the Fermi surface. The second effect is the addition of electrons to the bands, which, by itself, should tend to distort the Fermi surface more severely. An actual band calculation of alpha brass has not been carried out, so that the predictions of Cohen and Heine cannot be tested from first principles.

As we have seen, the conduction-band gaps of β'CuZn are smaller relative to those of Cu. The p-like levels are below the s-like levels as in the noble metal. Although the exact positions of the d bands are quite sensitive to the potential, they are considerably lower with respect to the Fermi energy than in the case of Cu, diminishing the importance of s-d hybridization and contributing to the reduction of p-s gaps. The nature of these results suggests their possible interpretation in the light of the Cohen-Heine theory extended to the limit of the alpha phase and onset of the beta phase. Within the narrow composition limits of the latter phase, the chief effect of adding Zn should be to fill the bands in rigid-band fashion. Muldawer's[31] composition-dependent optical data is consistent with this viewpoint.

Alpha brass is a true solid solution since it is stable over a wide range of solute concentration (0–36% Zn), or between the electron-to-atom ratios e/a of 1.0 and 1.36. On the other hand, beta brass is often called an electron compound because of its very narrow range of stability around the Hume-Rothery[40] ratio $e/a=1.5$. Jones[41] attempted to explain these ratios in terms of the free-electron model and the principle of minimum free energy. The 1.36 limit of the alpha phase was interpreted as occurring when the Fermi sphere contacts the {111} (hexagonal) faces of the octahedral Brillouin zone of the fcc structure. The 1.5 value for the beta phase was interpreted as occurring when the sphere touches the {110} faces of the dodecahedral zone. It is now understood that the Fermi surface of pure Cu is considerably anisotropic, already contacting the {111} faces of the octahedron. A more recent theory of the alpha-phase boundary is that some "sphericization" of the Fermi surface coupled with the filling of the bands as Zn is added to Cu should cause the surface to make contact with the {200} (square) faces of the zone near the e/a value of 1.36.

We have presented evidence that in ordered beta brass measurable contact of the Fermi surface with the faces of the dodecahedron takes place without severe distortion of the surface from the nearly free-electron or one-orthogonalized-plane-wave (OPW) case. Thus Jones' analysis appears to be correct for the β' phase. It is this contact which most likely triggers the transformation from the β' phase to the γ phase when one or two percent of Zn is added beyond the $\beta'Cu_{50}Zn_{50}$ composition. Although our theoretical analysis and most of the experimental data used are for the ordered alloy, much of what we have just said should be relevent to the stability of the high temperature disordered β phase. In this case, the first (cubic) zone is absent. The relatively small energy gap evident at the faces of the cube suggests that its complete absence should not critically alter the measured amount of contact of the Fermi surface with the faces of the dodecahedron, if one assumes that the one-electron model is meaningful in the case of disorder. Recent advances in theory, such as those due to Edwards[42] and to Phariseau and Ziman,[43] support the latter assumption, and furthermore, suggest the possibility of detailed theoretical treatment of a disordered alloy.

Note added in proof. Since the submission of the manuscript, we have received results of the APW band calculation of beta brass carried out by Arlinghaus of the MIT Quantum Theory Group. The conduction bands and Fermi surface agree well with the results of the Green's-function method. However, the Cu d bands lie higher than those obtained by our second choice of potential (Fig. 7). This discrepancy is due to the somewhat different potential used by Arlinghaus, adding testimony to the sensitivity of the relative positions of conduction and d bands to the exact nature of the potential.

ACKNOWLEDGMENTS

We wish to thank Dr. F. S. Ham, Dr. W. Piper, and Dr. B. Segall of the General Electric Research Laboratory for the use of their unpublished calculations. For their advice and assistance in programming the computations, we are grateful to Dr. S. Weintraub of the Applied Data Research Company of Princeton, and J. McLaughlin of the Temple University Computing Center. It is a pleasure to acknowledge the hospitality received both at this computing center and at that of the Courant Institute of New York University. We wish to thank Dr. L. Muldawer of Temple for his helpful discussions of the optical properties, and also Dr. M. Springford, Dr. W. B. Pearson, Dr. J. P. Jan, and Dr. I. M. Templeton of National Research Council of Canada for correspondence concerning their de Haas–van Alphen results. Finally, we are very grateful to A. Karakashian for his assistance in performing the last phases of the computations.

[40] W. Hume-Rothery, J. Inst. Metals **35**, 309 (1926).
[41] H. Jones, Proc. Phys. Soc. (London) **49**, 243 (1937).
[42] S. F. Edwards, Proc. Roy. Soc. (London) **A267**, 518 (1962).
[43] P. Phariseau and J. M. Ziman, Phil. Mag. **8**, 1487 (1963).